Optical and acoustic plasmons in the layered material Sr_2RuO_4

J. Schultz,[1, *] A. Lubk,[1, 2] F. Jerzembeck,[3] N. Kikugawa,[4] M. Knupfer,[1] D. Wolf,[1] B. Büchner,[1, 2] and J. Fink[1, 2, †]

[1]*Leibniz Institute for Solid State and Materials Research Dresden, Helmholtzstraße 20, 01069 Dresden, Germany*
[2]*TU Dresden, Institute of Solid State and Materials Physics, Haeckelstraße 3, 01069 Dresden, Germany*
[3]*Max Planck Institute for Chemical Physics of Solids,*
Nöthnitzer Strasse 40, D-01187 Dresden, Germany
[4]*National Institute for Materials Science, Tsukuba 305-0003, Japan*
(Dated: January 12, 2024)

I. ABSTRACT

We use momentum-dependent electron energy-loss spectroscopy in transmission to study collective charge excitations in the "strange" layer metal Sr_2RuO_4. We cover a complete range between in-plane and out-of-plane oscillations. Outside of the classical range of electron-hole excitations, leading to a Landau damping, we observe well defined plasmons. The optical (acoustic) plasmon due to an in-phase (out-of-phase) charge oscillation of neighbouring layers exhibits a quadratic (linear) dispersion. Using a model for the Coulomb interaction of the charges in a layered system, it is possible to describe the complete range of plasmon excitations in a mean-field random phase approximation without taking correlation effects into account. There are no signs of over-damped plasmons predicted by holographic theories. This indicates that long wavelength charge excitations are not influenced by local correlation effects such as on-site Coulomb interaction and Hund's exchange interaction.

II. PLASMONS IN "STRANGE" METALS

"Strange" metals are at present one of the most interesting research fields in solid state physics. Due to the strong interaction between their charge carriers, they show a deviation from the Fermi-liquid behaviour revealed, e.g., by the linear temperature dependence of the electrical resistivity [1]. The unconventional and in some cases high-temperature superconductivity detected in these materials is supposed to be related to their "strange" normal state electronic structure. Doped cuprates and Sr_2RuO_4 above 30 K are prototypes of these "strange" metals.

There are various methods to study their electronic structure. Here we use electron energy-loss spectroscopy in transmission (T-EELS). We study the charge density-density response connected with plasmon excitations.

The interest in such collective electronic excitations has increased sharply. This can be associated with the emergence of new experimental methods. Resonant Inelastic X-ray Scattering (RIXS) [2, 3] has contributed a lot to our understanding of acoustic plasmons in layered materials such as various p- and n-type doped cuprates. High-resolution EELS in reflection (R-EELS) has opened up access to the examination of novel charge carrier excitations at very low energies and momentum [4]. Also, energy and momentum resolution in T-EELS could be significantly improved by advanced energy filter instrumentation [5]. Moreover, *in-situ* stimulation of the sample could be extended. E.g., low temperatures could be reached in RIXS, T-EELS, and R-EELS experiments incorporating liquid Helium cooling. Finally there is important progress in the preparation of single-crystalline thin films for T-EELS using focused ion beam preparation which is an important point in the present T-EELS study of Sr_2RuO_4.

Experimental studies were also stimulated by theoretical work [6, 7] which postulated that unconventional superconductivity is mediated by a coupling of the charge carriers to charge excitations in the small momentum regime. Great attention attracted the prediction of over-damped plasmons in "strange" metals and a replacement of these excitations by a continuum [8]. The authors concluded that a new kind of theory of strongly interacting matter may be needed to explain this continuum. The latter may also be connected to the phenomenon of high-T_c superconductivity. The over-damped plasmon was discussed in terms of holographic theories, which predicted, different from the classical Landau damping, a strong damping even for the long wavelength plasmons due to quantum critical fluctuations. Recently, this work was supported by similar calculations [9]. The existence of a low energy continuum is also the basis for the phenomenological model of the marginal Fermi liquid which describes the linear in energy/temperature scattering rate [10].

The theoretical predictions of an over-damped plasmon are in stark conflict with early T-EELS studies on cuprates. A well defined dispersive plasmon was detected in $Bi_2Sr_2CaCu_2O_8$, using T-EELS [11–13]. Also, in various cuprates, well pronounced dispersive acoustic plasmons were detected by RIXS [2, 3, 14].

Recently, we have studied the electronic structure of Sr_2RuO_4 [15] by an investigation of the optical plasmon

* j.schultz@ifw-dresden.de
† j.fink@ifw-dresden.de

excitations parallel to the layers [16] using a dedicated T-EELS spectrometer [17]. Also in this highly correlated material, a well defined plasmon could be detected near 1.5 eV. The plasmon has a positive dispersion and decays into a continuum of particle-hole excitations due to Landau damping, which could be explained in the framework of the random phase approximation (RPA).

On the other hand, there are several recent experimental R-EELS studies, supporting the theories which predict over-damped plasmons in "strange" metals. In $Bi_2Sr_2CaCu_2O_8$ and in Sr_2RuO_4, only at very small momentum a well defined plasmon exists followed by a transition into a featureless momentum-independent continuum [18–20].

Most of the previous momentum dependent EELS studies on layered materials were performed for a wave vector parallel to the layers. The reason for this is that thin samples (T-EELS) or clean surfaces (R-EELS) are easily prepared by a cleavage of the crystals parallel to the layers. In the present work, by focused ion beam milling, we are able to prepare thin electron transparent lamella in which the layers are perpendicular to the surface. Using such samples, it was for the first time possible to map out a complete set of plasmon excitations with momentum between parallel and perpendicular to the layers almost in the entire Brillouin zone (BZ). In this way, it is possible to control theoretical work on plasmon excitations in layered compounds which is available since many decades [21–24].

III. PLASMON DISPERSION IN LAYERED SYSTEMS

The dynamic structure factor is determined by the Fourier transformation of the charge density-density correlation function. It can be expressed [25] by the dynamical susceptibility $\chi(\mathbf{q}, \omega)$:

$$S(\mathbf{q}, \omega) \propto \Im\left[\chi(\mathbf{q}, \omega)\right] \propto \Im\left[-\frac{1}{\epsilon(\mathbf{q}, \omega)}\right]. \quad (1)$$

Here, $\epsilon(\mathbf{q}, \omega)$ is the complex dielectric function.

The calculation of the susceptibility of the many-body system of the charge carriers in solids is a challenging task. The susceptibility χ_0 for a non-interacting one-band electron liquid is given by [26]:

$$\chi_0(\omega, \mathbf{q}) = \int_{\mathrm{BZ}} A(\mathbf{q}, \mathbf{k}) \frac{2F(\mathbf{k})\Delta E(\mathbf{q}, \mathbf{k})}{(\omega + i\Gamma)^2 - \Delta E^2(\mathbf{q}, \mathbf{k})} d^3k. \quad (2)$$

Here $\Delta E = E_{\mathbf{k}+\mathbf{q}} - E_{\mathbf{k}}$, $E_{\mathbf{k}}$ are the band energies of the electrons having a momentum $\mathbf{k}$, $A(\mathbf{q}, \mathbf{k})$ is related to matrix elements, Γ is the lifetime broadening of the particle-hole excitations, and $F(\mathbf{k})$ is the Fermi function.

While χ_0 is the susceptibility related to an external field, stemming from the field of the scattering electron, χ is the susceptibility for the total field, including the induced one. Running a self-consistency (SC) cycle, we obtain the mean field RPA result:

$$\chi^{\mathrm{SC}}(\mathbf{q}, \omega) = \frac{\chi_0(\mathbf{q}, \omega)}{1 - V(\mathbf{q})\chi_0(\mathbf{q}, \omega)}. \quad (3)$$

Here, $V(\mathbf{q})$ is the Fourier transformed Coulomb interaction.

In this approximation and for small damping, there are in addition to the single-particle excitations collective excitations, termed plasmons. The energy of the plasmon is determined by the zeros of the real part of the denominator of Eq. (3). The long wavelength energy of the plasmon in the RPA is given by

$$\omega_{\mathrm{P}}(0)^2 = \frac{4\pi Ne^2}{m} \quad (4)$$

with N being the density of the charge carriers, and m their mass.

For small but finite momentum, the charge density has to be compressed and therefore the plasmon exhibits a positive dispersion, which within the RPA is given by

$$\omega_{\mathrm{P}}(q)^2 = \omega_{\mathrm{P}}(0)^2 + A_{\mathrm{RPA}}q^2; \quad A_{\mathrm{RPA}} = \frac{3}{5} < v_{\mathrm{F}}^2 >_{\mathbf{q}} \quad (5)$$

where $< v_{\mathrm{F}}^2 >_{\mathbf{q}}$ is the average squared Fermi velocity along the $\mathbf{q}$ direction. When the plasmon merges into the single-particle continuum, it decays into particle-hole excitations. This process is termed Landau damping.

In the following we discuss the structure factor $V(\mathbf{q})$. In a homogeneous electron system

$$V(\mathbf{q}) = \frac{4\pi e^2}{q^2}. \quad (6)$$

For a system, built up by 2D layers separated by the distance d we use the Fetter model with the Coulomb potential

$$V(\mathbf{q}) = V(q_{||}, q_\perp) = \frac{4\pi e^2}{q^2} \frac{q_{||}d}{2} \frac{\sinh(q_{||}d)}{\cosh(q_{||}d) - \cos(q_\perp d)}, \quad (7)$$

where $q_{||}(q_\perp)$ is the momentum parallel (perpendicular) to the layer [22]. In a layer system the plasmon dispersion is not only determined by the compressibility of the electron liquid (see Eq. 5) but also by the structure factor $V(\mathbf{q})$:

$$\omega_{\mathrm{P}}(q)^2 = A_{\mathrm{RPA}}q_{||}^2 + \omega_{\mathrm{P}}(0)^2 \frac{q_{||}d}{2} \frac{\sinh(q_{||}d)}{\cosh(q_{||}d) - \cos(q_\perp d)}. \quad (8)$$

For small $q_{||}$ and $q_\perp d = 0$ or, the structure factor $V(q_{||}, q_\perp)$ is the same as in the homogeneous electron gas. In this case, the charge oscillations in the layers are in phase and the plasmon dispersion is the same as in a homogeneous 3D electron system. For $q_\perp d = \pi$ the charge oscillations between neighboring layers are out of phase.

This leads to an acoustic plasmon, without energy offset. The dispersion of the acoustic plasmon for small $q_{||}$ is given by

$$\omega_{\mathrm{p}}(q_{||}) = q_{||}\sqrt{\frac{3}{5} < v_{\mathrm{F}}^2 >_{\mathrm{q}} + \omega_{\mathrm{p}}(0)^2 \frac{d^2}{4}}. \qquad (9)$$

Very often, the first term in the square root is considerably smaller than the second. Then the phase velocity of the acoustic plasmon along the direction of $q_{||}$ is given by

$$v_{\mathrm{p}} = \frac{\omega_{\mathrm{p}}(0)d}{2}. \qquad (10)$$

IV. EELS DATA

T-EELS measurements were performed on single-crystalline Sr_2RuO_4 layers at room temperature. Fig. 1 shows the crystal structure of Sr_2RuO_4 which consists of RuO_2 layers along the **c**-axis direction together with SrO spacer layers. The thin films were characterized by *in-situ* elec-
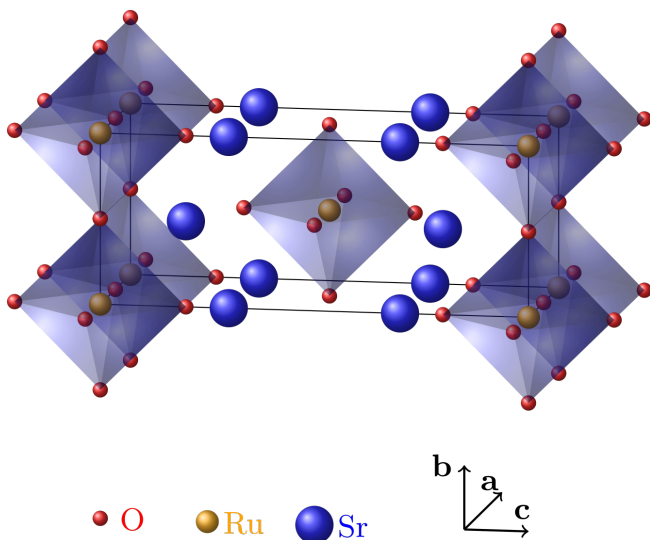

FIG. 1. Crystal structure of Sr_2RuO_4.

tron diffraction and the crystallographic axes were oriented with respect to the $(\mathbf{a}, \mathbf{c})$ plane. The distance $d = 6.36$ Å between the RuO_2 layers is half the **c**-axis lattice constant. The thin lamellas for T-EELS with a normal direction parallel to the **b**-axis were cut with a focused ion beam. In this way, EELS experiments were possible with the momentum parallel to the $(\mathbf{a}, \mathbf{c})$ plane. We emphasize that this momentum range is different from our previous EELS study on Sr_2RuO_4 [16] where we covered the momentum range parallel to the **a**-axis. The thin films were characterized by *in-situ* electron diffraction and the crystallographic axes were oriented with respect to the transferred momentum [see Fig. 2 (a)].

T-EELS was performed with a primary electron energy of 80 keV and with an energy and momentum resolution

of 120 meV and 0.04 Å^{-1}, respectively. The EELS data were sequentially recorded with fixed momentum transfer in the $(q_{\mathrm{a}}, q_{\mathrm{c}})$ momentum plane as depicted in Fig. 2(b). In Fig. 3 we show typical EELS intensities (red lines) as
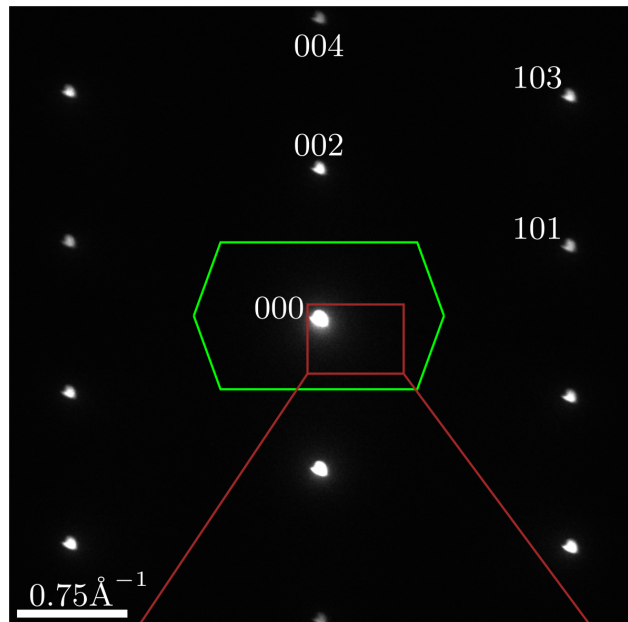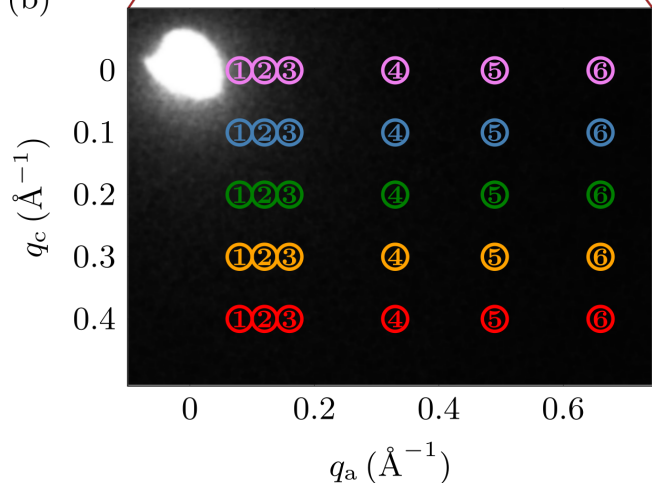

FIG. 2. (a) Indexed electron diffraction pattern (white dots) in the $(q_{\mathrm{a}}, q_{\mathrm{c}})$ plane including the reduced Brillouin zone (green) for equal layers along the **c**-axis. (b) Brown momentum range [see (a)] in which loss spectra are recorded for various q_{a} and q_{c} values. The colours purple, blue, green, yellow, and red correspond to q_{c} equal 0, 0.1, 0.2 0.3, and 0.4 Å^{-1}, respectively. The diameter of the filter entrance aperture [indicated by the colored circles in (b)] corresponds to a momentum of 0.041 Å^{-1}.

a function of the energy for various q_{a} and q_{c} values. With increasing q_{a} the plasmon energy slightly increases whereas for increasing q_{c} the plasmon energies decrease.

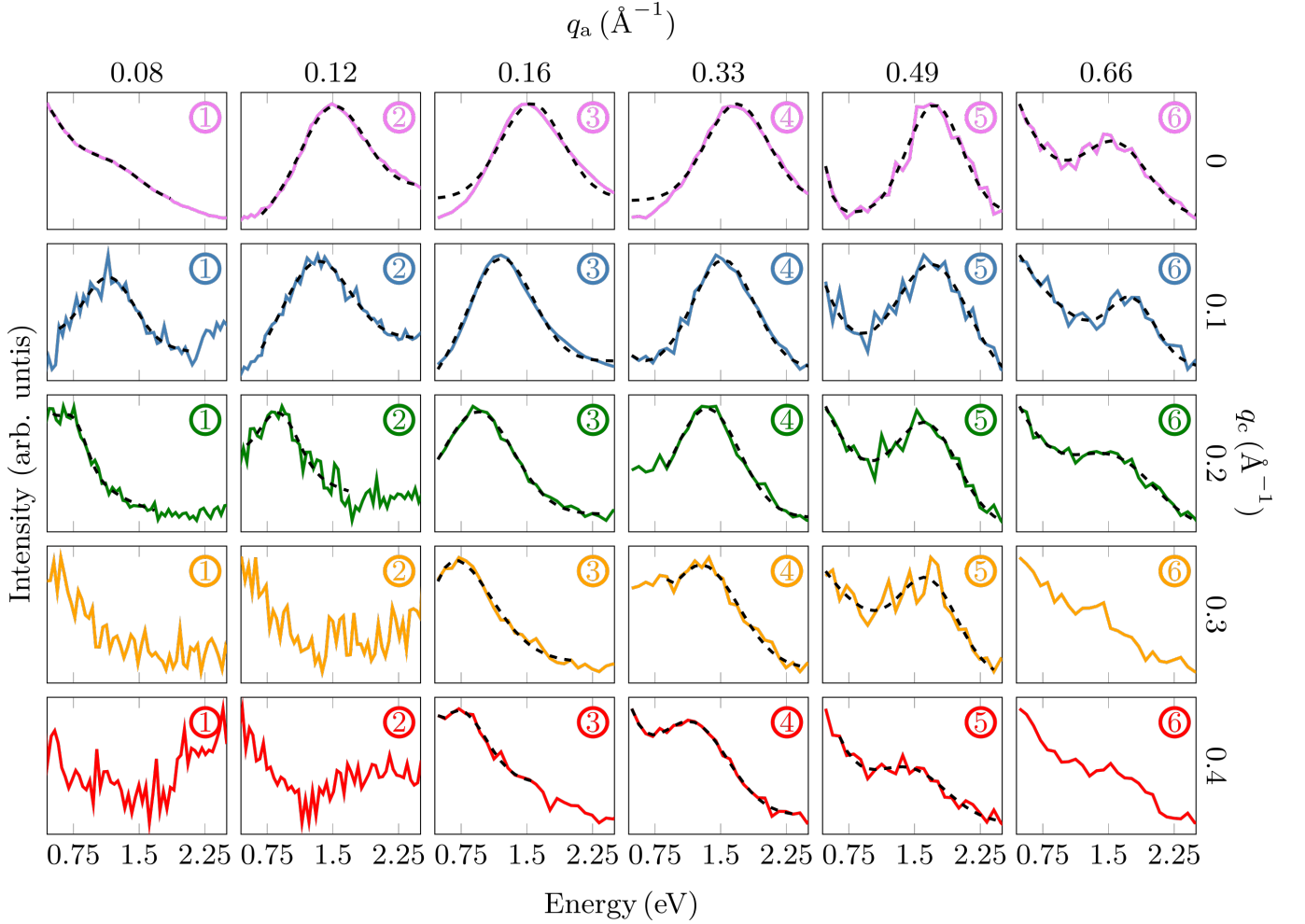At low total momentum it is difficult to see a well de-

FIG. 3. Electron energy-loss intensities for various q_a and q_c values. The numbers and the colours correspond to the momentum values depicted in Fig. 2. Coloured lines: experimental intensities. The black dashed lines are fits of a Lorentzian on top of an exponential background due to the tails of the quasi-elastic peak at zero energy.

fined plasmon due to the high intensity of the quasi-elastic peak. The same holds for high total momentum because the T-EELS cross section is decreasing with $1/q^2$. Except for the described cases, well developed and dispersing plasmon excitations below 1.8 eV are visible. From the fit to the data we obtain the energy of the plasmon excitations.

The latter is plotted in Fig. 4 as a function of q_a for various q_c values together with theoretical curves calculated in the framework of the Fetter model (see Section III). We use the parameters $\omega_p(0) = 1.48$ eV (from optical spectroscopy [27], $d = 6.36$ Å, and $< v_F^2 >_{100} = 4.91$ (eV Å)^2. The latter value for the three Ru 4d t_{2g} bands crossing the Fermi level was derived from a tight-binding (TB) band structure [28] (see Methods). For all plasmon energies above the continuum, within error bars, there is rather good agreement between theory and experiment. There is a continuous transition between the optical plasmon for $q_c = 0$ (purple data) at higher energy to the acoustic plasmon ($q_c = 0.4$ Å^{-1}) close to $q_c = \pi/d = 0.49$

Å^{-1} (red data) at lower energy. Due to our finite energy resolution we cannot follow the acoustic plasmon to zero energy. The rapid decay in the theoretical curve for the optical plasmon near $q_c = 0$ is due to the finite momentum resolution, i.e., integration of optical and acoustic plasmons within the EEL collection aperture. The difference between RPA dispersion and experimental data for $q_a \geq q_{crit}$ can be explained by Landau damping. A similar behavior has been also observed for Al [29]. In Fig. 4 we also show the continuum of the single-particle intraband transitions χ_0 (see the grey region) calculated using an unrenormalized TB band structure [28] (see Methods). The optical plasmon merges into the continuum near $q_a = 0.45$ Å^{-1}. We assign this value to the critical momentum q_{crit}. This value was also derived in Ref. [16] from the rapid increase of the plasmon width at this wave vector.
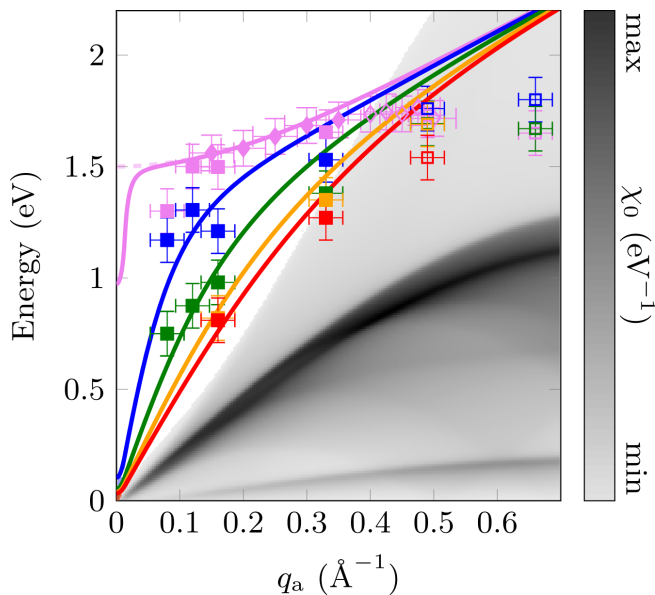
FIG. 4. Plasmon dispersion along the momentum q_a parallel to the layers for several q_c perpendicular to the layers (squares) together with calculations within the framework of the Fetter model (solid lines). The q_c values 0, 0.1, 0.2, 0.3, and 0.4 Å^{-1} are marked by purple, blue, green, yellow, and red colour squares, respectively (see Fig. 3). We have added also the data from the optical plasmon dispersion derived in our previous publication (purple diamonds) [16]. The horizontal error bars originate from the finite momentum resolution while the vertical ones are related to energy error bars. The region marked in grey corresponds to the susceptibility χ_0 calculated from a tight binding band structure (see Methods). The excitations in the continuum range are marked by open symbols.

V. OPTICAL AND ACOUSTIC PLASMONS IN LAYERED "STRANGE" METALS

The data presented in Fig. 3 demonstrate that T-EELS is capable to study not only optical plasmons with momentum parallel to the layers. Using a suitable sample preparation, we have demonstrated that it is also possible to cover the complete momentum range parallel and perpendicular to the layers, i.e., in-phase (optical) and out-of phase (acoustic) collective charge oscillations in neighboring layers. Thus, we show that T-EELS can compete with recent RIXS studies of acoustic plasmons of cuprates [2, 3, 30]. This will be even possible to perform at lower energies when T-EELS spectrometers will be available with high energy resolution in the near future. This is an important extension of T-EEL spectroscopy. Furthermore, we emphasize that the present work shows that acoustic plasmons exist also in noncuprate "strange" metal layer systems.

Well defined plasmon exist in the complete range which is not covered by the range of single-particle particle excitations calculated in the mean-field RPA theory. Optical plasmons exist in ≈ 15 % of the BZ. The rest is

determined by a continuum of intra-band single particle excitations. There is no sign of a reduction of the coherent plasmon range due to an over-damping discussed in terms of holographic theories [8, 9].

In the following we compare the present EELS results with theoretical predictions in a more quantitative way. In our previous publication we analyzed the plasmon dispersion by a calculation of the susceptibility together with an adjustment of the strength of the Coulomb potential to $\omega_P(0)$. The comparison with the experimental dispersion yields good agreement when using an unrenormalized TB band structure ($\frac{m^*}{m_0} = 1$) instead of a renormalized band structure with an effective mass $\frac{m^*}{m_0} \approx 4.5$ taken from angle-resolved photoemission spectroscopy (ARPES) experiments [31]. In this quite indirect analysis, we concluded that the plasmon dispersion is not influenced by the mass renormalization observed by ARPES.

Here we perform a similar, but much more direct analysis. Fitting the dispersion of the optical plasmon dispersion for $q \leq q_{crit} \approx 0.45$ Å^{-1} (see Fig. 4 purple data) with Eq. (1) we derive a dispersion coefficient $A = 1.8 \pm 0.8$ (eVÅ)^2 which is in agreement with the more precise result from our previous publication $A = 2.1 \pm 0.2$ (eVÅ)^2. Using the unrenormalized TB band structure [28] we receive a squared Fermi velocity $< v_F^2 >_{100} = 3.4$ (eVÅ)^2 and the dispersion coefficient $A = 2.5$ (eVÅ)^2. The latter value is close to the experimental value. On the other hand, using the effective mass $\frac{m^*}{m_0} \approx 4.5$ from ARPES [31] we derive a dispersion coefficient $A = 0.1$ (eVÅ)^2 which is at variance with the experimental data. Thus our present and the previous experimental data of the dispersion of the optical plasmon indicates that the long wavelength dispersion can be explained in the framework of a mean-field RPA theory.

It is also interesting to realize that the detected critical wave-vector q_{crit} agrees well with the calculated susceptibility (see Fig. 4), although the latter was calculated with an unrenormalized TB band structure. This may be related to the observation of a decreasing effective mass with increasing energy and the formation of resilient quasi-particles [27].

In the following we discuss the acoustic plasmon data (see red data and line in Fig. 4). Despite the gap at low energy due to a finite energy resolution, the dispersion extrapolates to zero energy typical of an acoustic plasmon. The derived experimental plasmon velocity is $v_P \approx 4.7$ eVÅ. From Eq. (9) we derive $v_P \approx 4.8$ eVÅ in very good agreement with the experimental value. This indicates that the first term in Eq. (9) due to the finite Fermi velocity is small compared to the term which only depends on $\omega_P(0)$ and d. Thus, for a given $\omega_P(0)$ the acoustic plasmon dispersion only depends on d and is not influenced by many-body interactions.

Neglecting the Fermi velocity term, the linear acoustic plasmon dispersion [see Eq. (9)] can be explained in the following way. The phase difference π of the oscillations between neighboring layers reduces the plasmon energy

from $\omega_P(0)$ to zero. When adding a momentum q_a the phase difference between neighboring layers is increased to $\pi + q_a d$ and therefore, using a linear relation, the energy of the acoustic plasmon should increase by $(\omega_p(0) d q_a)/\pi$ which is close to Eq. (10).

In summary, the long wavelength q_a dispersion of the q_c dependent plasmons including the optical and the acoustic collective excitations and the decay of the optical plasmon by Landau damping can be all explained in terms of a mean-field RPA model. It is possible to understand this interpretation of the present results in the following way. Long wavelength charge excitations are not influenced by local interactions such as on-site Coulomb and Hund's exchange interactions. This behaviour is different from ARPES studies, in which local properties play an important role. In this context it is also important to note that mono-pole (a single hole) excitations detected in ARPES are differently screened compared to dipole excitations recorded in EELS. We further emphasize that our present analysis of the acoustic plasmon dispersion is also important for the understanding of previous [2, 3, 30] and future RIXS studies on cuprates.

VI. PERSPECTIVES

The present study has demonstrated that optical and acoustic plasmons can be investigated by T-EELS in the complete BZ in layered systems. Therefore, with the advent of higher energy resolution, T-EELS will be competitive at lower energies with RIXS, also taking into account that momentum-resolved T-EELS provides a direct probe of the dynamic susceptibility. Then, in "strange" metals, it will be possible to study low-energy and high-momentum charge excitations which were predicted in Ref. [32] to depend on correlation effects. In this way it will be possible to study the spacial dependence of the density-density fluctuations in "strange" metals.

VII. METHODS

A. Samples

Sr_2RuO_4 crystals were grown using the floating-zone method [33]. The superconducting transition tempera-

ture of the sample was $T_c = 1.5$ K.

Thin TEM lamellas of Sr_2RuO_4 with the normal pointing along **b** were prepared by Focused Ion Beam (FIB) using a Thermofisher instrument. The target thickness of the lamellas was 80 nanometers. Low ion energy polishing was used as final step to thin Ga-ion damaged surface layers.

B. EELS measurements

The momentum-resolved loss function was recorded at a FEI Titan[3] TEM equipped with a Wien monochromator and a Gatan Tridiem imaging filter (GIF) at 80 kV acceleration voltage in a serial way (i.e., one EEL spectrum per fixed momentum). The energy resolution is around $120\,\mathrm{meV}$ (FWHM of zero loss peak). Using a camera length (i.e., effective distance between sample and detector) of $1.15\,\mathrm{m}$. The GIF entrance aperture was used to select the different momentum values and covers a momentum range of $0.04\,\text{Å}^{-1}$. Due to instabilities of the monochromator and the rather long collection times required at large momentum transfers, the recorded spectra are subject to substantial noise as well as mutual random fluctuations/offsets. In order to mitigate these effects, each spectrum was separately aligned with the help of the quasi-elastic peak. Subsequently the quasi-elastic peak was subtracted (the peak was obtained by reflecting the gain tail at zero loss energy), before analyzing the position of the plasmon peak.

C. Fermi velocities and susceptibility

For the calculation of the Fermi velocity along the [100] direction and the bare particle susceptibility $\chi_0(q_a, 0, \omega)$ we used a TB band structure [28] based on a LDA band structure. We use a multi-band version of Eq. 2 and taking only intra-band excitations into account with the same matrix element, thus neglecting inter-band excitations. Mainly the β and the γ bands contribute to $< v_F^2 >_{100}$ and χ_0.

VIII. REFERENCES

[1] R. A. Cooper, Y. Wang, B. Vignolle, O. J. Lipscombe, S. M. Hayden, Y. Tanabe, T. Adachi, Y. Koike, M. Nohara, H. Takagi, C. Proust, and N. E. Hussey, Anomalous Criticality in the Electrical Resistivity of La$_{2-x}$Sr$_x$CuO$_4$, Science **323**, 603 (2009), https://www.science.org/doi/pdf/10.1126/science.1165015.

[2] M. Hepting, L. Chaix, E. W. Huang, R. Fumagalli, Y. Y. Peng, B. Moritz, K. Kummer, N. B. Brookes, W. C. Lee, M. Hashimoto, T. Sarkar, J.-F. He, C. R. Rotundu, Y. S. Lee, R. L. Greene, L. Braicovich, G. Ghiringhelli, Z. X. Shen, T. P. Devereaux, and W. S. Lee, Three-dimensional collective charge excitations in electron-doped copper oxide superconductors, Nature **563**, 374 (2018).

[3] A. Nag, M. Zhu, M. Bejas, J. Li, H. C. Robarts, H. Yamase, A. N. Petsch, D. Song, H. Eisaki, A. C. Walters, M. García-Fernández, A. Greco, S. M. Hayden, and K.-J. Zhou, Detection of acoustic plasmons in hole-doped lanthanum and bismuth cuprate superconductors using res-

onant inelastic x-ray scattering, PRL **125**, 257002 (2020).

[4] S. Vig, A. Kogar, M. Mitrano, A. Husain, L. Venema, M. Rak, V. Mishra, P. Johnson, G. Gu, E. Fradkin, M. Norman, and P. Abbamonte, Measurement of the dynamic charge response of materials using low-energy, momentum-resolved electron energy-loss spectroscopy (m-eels), SciPost Phys. **3**, 026 (2017).

[5] O. L. Krivanek, T. C. Lovejoy, N. Dellby, T. Aoki, R. W. Carpenter, P. Rez, E. Soignard, J. Zhu, P. E. Batson, M. J. Lagos, R. F. Egerton, and P. A. Crozier, Vibrational spectroscopy in the electron microscope, Nature **514**, 209 (2014).

[6] J. Ruvalds, Plasmons and high-temperature superconductivity in alloys of copper oxides, PRB **35**, 8869 (1987).

[7] V. Z. Kresin and H. Morawitz, Layer plasmons and high-T_c superconductivity, PRB **37**, 7854 (1988).

[8] A. Romero-Bermúdez, A. Krikun, K. Schalm, and J. Zaanen, Anomalous attenuation of plasmons in strange metals and holography, PRB **99**, 235149 (2019).

[9] S. T. V. den Eede, T. J. N. van Stralen, C. F. J. Flipse, and H. T. C. Stoof, Plasmons in a layered strange metal using the gauge-gravity duality (2023), arXiv:2311.03142 [cond-mat.str-el].

[10] C. M. Varma, P. B. Littlewood, S. Schmitt-Rink, E. Abrahams, and A. E. Ruckenstein, Phenomenology of the normal state of cu-o high-temperature superconductors, PRL **63**, 1996 (1989).

[11] N. Nücker, H. Romberg, S. Nakai, B. Scheerer, J. Fink, Y. F. Yan, and Z. X. Zhao, Plasmons and interband transitions in $bi_2sr_2cacu_2o_8$, PRB **39**, 12379 (1989).

[12] Y.-Y. Wang, G. Feng, and A. L. Ritter, Electron-energy-loss and optical-transmittance investigation of $bi_2sr_2cacu_2o_8$, Phys. Rev. B **42**, 420 (1990).

[13] N. Nücker, U. Eckern, J. Fink, and P. Müller, Long-wavelength collective excitations of charge carriers in high-tc superconductors, Phys. Rev. B **44**, 7155 (1991).

[14] A. Singh, H. Y. Huang, C. Lane, J. H. Li, J. Okamoto, S. Komiya, R. S. Markiewicz, A. Bansil, T. K. Lee, A. Fujimori, C. T. Chen, and D. J. Huang, Acoustic plasmons and conducting carriers in hole-doped cuprate superconductors, Phys. Rev. B **105**, 235105 (2022).

[15] Y. Maeno, H. Hashimoto, K. Yoshida, S. Nishizaki, T. Fujita, J. G. Bednorz, and F. Lichtenberg, Superconductivity in a layered perovskite without copper, Nature **372**, 532 (1994).

[16] M. Knupfer, F. Jerzembeck, N. Kikugawa, F. Roth, and J. Fink, Propagating charge carrier plasmons in sr_2ruo_4, Phys. Rev. B **106**, L241103 (2022).

[17] J. Fink, Adv. Electr. Electr. Phys. **75**, 121 (1989).

[18] M. Mitrano, A. A. Husain, S. Vig, A. Kogar, M. S. Rak, S. I. Rubeck, J. Schmalian, B. Uchoa, J. Schneeloch, R. Zhong, G. D. Gu, and P. Abbamonte, Anomalous density fluctuations in a strange metal, Proc Natl Acad Sci USA **115**, 5392 (2018).

[19] A. A. Husain, M. Mitrano, M. S. Rak, S. Rubeck, B. Uchoa, K. March, C. Dwyer, J. Schneeloch, R. Zhong, G. D. Gu, and P. Abbamonte, Crossover of charge fluctuations across the strange metal phase diagram, PRX **9**, 041062 (2019).

[20] A. A. Husain, E. W. Huang, M. Mitrano, M. S. Rak, S. I. Rubeck, X. Guo, H. Yang, C. Sow, Y. Maeno, B. Uchoa, T. C. Chiang, P. E. Batson, P. W. Phillips, and P. Abbamonte, Pines' demon observed as a 3d acoustic plasmon in sr2ruo4, Nature 10.1038/s41586-023-06318-8 (2023).

[21] D. Grecu, Plasma frequency of the electron gas in layered structures, PRB **8**, 1958 (1973).

[22] A. L. Fetter, Electrodynamics of a layered electron gas. ii. periodic array, Annals of Physics **88**, 1 (1974).

[23] S. Das Sarma and J. J. Quinn, Collective excitations in semiconductor superlattices, Phys. Rev. B **25**, 7603 (1982).

[24] A. Greco, H. Yamase, and M. Bejas, Plasmon excitations in layered high-T_c cuprates, Phys. Rev. B **94**, 075139 (2016).

[25] P. M. Platzman and P. A. Wolff, *Waves and Interactions inSolid State Plasmas* (Academic Press, New York, 1973).

[26] H. Ehrenreich and M. H. Cohen, Self-consistent field approach to the many-electron problem, Phys. Rev. **115**, 786 (1959).

[27] D. Stricker, J. Mravlje, C. Berthod, R. Fittipaldi, A. Vecchione, A. Georges, and D. van der Marel, Optical response of sr_2ruo_4 reveals universal fermi-liquid scaling and quasiparticles beyond landau theory, PRL **113**, 087404 (2014).

[28] A. Liebsch and A. Lichtenstein, Photoemission quasiparticle spectra of sr_2ruo_4, Phys. Rev. Lett. **84**, 1591 (2000).

[29] P. Batson and J. Silcox, Experimental energy-loss function, im [- 1 ε (q, ω)], for aluminum, Physical Review B **27**, 5224 (1983).

[30] M. Hepting, M. Bejas, A. Nag, H. Yamase, N. Coppola, D. Betto, C. Falter, M. Garcia-Fernandez, S. Agrestini, K.-J. Zhou, M. Minola, C. Sacco, L. Maritato, P. Orgiani, H. I. Wei, K. M. Shen, D. G. Schlom, A. Galdi, A. Greco, and B. Keimer, Gapped collective charge excitations and interlayer hopping in cuprate superconductors, Phys. Rev. Lett. **129**, 047001 (2022).

[31] A. Tamai, M. Zingl, E. Rozbicki, E. Cappelli, S. Riccò, A. de la Torre, S. McKeown Walker, F. Y. Bruno, P. D. C. King, W. Meevasana, M. Shi, M. Radović, N. C. Plumb, A. S. Gibbs, A. P. Mackenzie, C. Berthod, H. U. R. Strand, M. Kim, A. Georges, and F. Baumberger, High-resolution photoemission on sr2ruo4 reveals correlation-enhanced effective spin-orbit coupling and dominantly local self-energies, Phys. Rev. X **9**, 021048 (2019).

[32] G. Khaliullin and P. Horsch, Theory of the density fluctuation spectrum of strongly correlated electrons, Phys. Rev. B **54**, R9600 (1996).

[33] J. S. Bobowski, N. Kikugawa, T. Miyoshi, H. Suwa, H. shu Xu, S. Yonezawa, D. A. Sokolov, A. P. Mackenzie, and Y. Maeno, Improved single-crystal growth of sr2ruo4, Condensed Matter **4**, 6 (2019).

IX.   DATA AVAILABILITY

All data supporting the findings are provided as figures in the article. Data files for all figures and accompanying tables are available from the corresponding authors on request.

ACKNOWLEDGMENTS

X.   AUTHOR CONTRIBUTIONS

J.F., M.K., A.L., and B.B. conceived the experiment, J.S. and D.W. performed the EELS experiment. J.S. and J.F. analyzed the data. F.J. and N.K. prepared and characterized the samples. J.F. calculated the susceptibility. J.F., J.S, and A.L. wrote the manuscript with input from all authors.